

Dynamical Quantum Anomalous Hall Effect in Strong Optical Fields

Woo-Ram Lee and Wang-Kong Tse

Department of Physics and Astronomy, The University of Alabama, Alabama 35487, USA
Center for Materials for Information Technology,
The University of Alabama, Alabama 35401, USA

(Dated: February 28, 2021)

Topological insulators (TIs) are characterized by the quantum anomalous Hall effect (QAHE) on the topological surface states under time-reversal symmetry breaking. Motivated by recent experiments on the magneto-optical effects induced by the QAHE, we develop a theory for the dynamical Hall conductivity for subgap optical frequency and intense optical fields using the Keldysh-Floquet Green's function formalism. Our theory reveals a nonlinear regime in which the Hall conductivity remains close to $e^2/2h$ at low frequencies. At higher optical fields, we find that the subsequent collapse of the half quantization is accompanied by coherent oscillations of the dynamical Hall conductivity as a function of field strength, triggered by the formation of Floquet subbands and the concomitant inter-subband transitions.

PACS numbers:

Introduction.— Topological quantum phases of matter are one of the most intriguing paradigms in contemporary condensed matter physics [1, 2]. Recently, intensive researches have been focused on the interplay between topological order and dynamics. This is well exemplified by the dynamical synthesis and manipulation of topological quantum phases, which include Floquet Chern insulators [3], Floquet TIs [4], Floquet Majorana fermions [5, 6], and Floquet Weyl semimetals [7, 8].

Topological Hall quantization is a hallmark signature of two-dimensional (2D) quantum anomalous Hall insulators [9]. The crucial ingredients to realize the quantum anomalous Hall state are strong spin-orbit coupling and a magnetic Zeeman gap Δ . With magnetic doping, these can be realized on the TI surface [10], single-layer or bilayer graphene [11, 12], and HgTe quantum well [13]. Under a *D.C.* bias, a robust Hall plateau corresponding to the quantized Hall value has already been observed [14–16] in magnetically doped TI films. While topological transport as a property of linear response has been extensively studied under a *D.C.* or an *A.C.* electric field serving as a weak probe field, one is naturally led to consider whether nonlinear responses can exhibit topological properties under strong optical pump fields. In this vein, recent works have shown that the second and third order optical susceptibilities [17–20] in topological matter may also contain topological contributions arising from a nonzero Berry curvature. An important unanswered question in the emerging topic of nonequilibrium topological response concerns the strong-field influences on the topological Hall conductivity. Theoretical predictions [21, 22] have shown that the quantization of the Hall conductivity can manifest as quantization of magneto-optical Faraday and Kerr rotations when TI thin films are illuminated by a low-frequency optical probe field, as confirmed in recent experiments [23–25]. This provides a strong motivation to consider the effects on the topological Hall quantization due to a strong *A.C.* driving

field E , particularly in the low-frequency subgap regime ($\hbar\Omega \ll \Delta$), when the light-matter interaction $\sim E/\Omega$ is manifestly nonperturbative.

In this work, we develop a theory for the dynamical Hall effect in quantum anomalous Hall insulators using the Keldysh-Floquet Green's function formalism. We note that the study of topological states using the Floquet formalism (in Floquet TIs, for example) has so far been largely focused on the high-frequency, off-resonance regime; the effects of low-frequency *A.C.* driving in the adiabatic regime, where the frequency is small compared to either the bandwidth or the band gap, remain not well understood. To remedy this situation, we numerically study the Hall conductivity as a function of the optical field strength and frequency without any expansion in powers of optical field strength. This approach allows us to address the full nonperturbative effects of the optical field on the electronic bands and transport properties of the system, even at low frequencies. For concreteness, we take the massive Dirac model describing TI surface states with broken time-reversal symmetry [26, 27] as our prototypical system of investigation. We expect the conclusions from our theory to be broadly applicable to other materials that host massive Dirac fermions such as Chern insulators and graphene-like materials with broken spatial-inversion symmetry.

2D massive Dirac fermions and QAHE.— We consider the quantum anomalous Hall state realized on the surface of a TI film with broken time-reversal symmetry, *e.g.*, by interfacing with a magnetic substrate or by doping with magnetic adatoms [1, 2, 9]. The film is sufficiently thick so that tunneling between the top and bottom surface states can be ignored [28]. Focusing on a single surface, a low-energy electron at the Γ point in the Brillouin zone is described by the 2D massive Dirac Hamiltonian $\mathcal{H} = \sum_{\mathbf{k}} \psi_{\mathbf{k}}^{\dagger} \mathcal{H}_{\mathbf{k}} \psi_{\mathbf{k}}$ with $\mathcal{H}_{\mathbf{k}} = \mathbf{d}_{\mathbf{k}} \cdot \boldsymbol{\tau}$. Here, $\psi_{\mathbf{k}} = (c_{\mathbf{k}\uparrow}, c_{\mathbf{k}\downarrow})^T$ with $c_{\mathbf{k}\alpha}$ the electron annihilation operator with momentum $\hbar\mathbf{k}$ and spin $\alpha (= \uparrow, \downarrow)$, $\boldsymbol{\tau} = (\tau_x, \tau_y, \tau_z)$ consists of the

Pauli matrices, and $\mathbf{d}_{\mathbf{k}} = (v\hbar k_x, v\hbar k_y, m_0)$ with v being the Dirac velocity. In the presence of the Dirac mass m_0 , or equivalently, the band gap $\Delta (= 2m_0)$, which is generated by the exchange field due to the magnetic substrate or adatoms, the bulk energy spectrum for the surface state becomes insulating with the energy dispersion $\mathcal{E}_{\mathbf{k}} = |\mathbf{d}_{\mathbf{k}}| = [(v\hbar)^2(k_x^2 + k_y^2) + m_0^2]^{1/2}$ for the conduction band and $-\mathcal{E}_{\mathbf{k}}$ for the valence band. In the presence of a time-independent *D.C.* electric field, 2D massive Dirac fermions give rise to the QAHE consisting of a robust one-half quantization of the Hall conductance in units of $\sigma_0 = e^2/h$ due to the half-skyrmion configuration of $\hat{\mathbf{d}}_{\mathbf{k}}$ [9]: $\sigma_{xy}/\sigma_0 = (1/4\pi) \int d^2\mathbf{k} \hat{\mathbf{d}}_{\mathbf{k}} \cdot (\partial_{k_x} \hat{\mathbf{d}}_{\mathbf{k}} \times \partial_{k_y} \hat{\mathbf{d}}_{\mathbf{k}}) = \text{sgn}(m_0)/2$, where $\hat{\mathbf{d}}_{\mathbf{k}} = \mathbf{d}_{\mathbf{k}}/|\mathbf{d}_{\mathbf{k}}|$, and ‘sgn’ denotes the signum function.

Dynamical response to the optical field.— We now consider linearly polarized light illuminated in the normal direction to the surface of the TI film. Choosing the polarization direction along the x axis and the propagation direction along the z axis, the incident light with electric field amplitude E and frequency Ω is described by the vector potential $\mathbf{A}(t) = -(cE/\Omega)\zeta(t)\sin(\Omega t)\hat{x}$. Here, a switching protocol is encoded in the function $\zeta(t) = e^{t/\tau_s}\Theta(-t) + \Theta(t)$, with τ_s being a switch-on time scale and $\Theta(x)$ the step function, which satisfies $\zeta \rightarrow 0$ for an equilibrium state at $t \rightarrow -\infty$ and $\zeta = 1$ for a nonequilibrium steady state (NESS) at $t \geq 0$. In the semiclassical treatment of the optical field, the Peierls substitution $\hbar\mathbf{k} \rightarrow \hbar\mathbf{k} + e\mathbf{A}(t)/c$ in the original Hamiltonian leads to the time-dependent Hamiltonian $\mathcal{H}_{\mathbf{k}}(t) = \mathcal{H}_{\mathbf{k}} + \mathcal{V}(t)$, with the perturbation of the form $\mathcal{V}(t) = -\mathcal{V}_0\zeta(t)\sin(\Omega t)\tau_x$ with $\mathcal{V}_0 = eEv/\Omega$ playing the role of Rabi frequency of the two-band system. The relative strength of the Rabi frequency to the photon energy defines the dimensionless coupling parameter $\lambda = \mathcal{V}_0/\hbar\Omega$, according to which the system is in a regime commonly classified as weak coupling ($\lambda \ll 1$) and strong coupling ($\lambda \gtrsim 1$) [29, 30] in quantum optics.

For the purpose of formulating a nonperturbative theory of dynamical response, we start with a generic form of the surface electric current density, $\mathbf{J}(t) = -eS^{-1}\sum_{\mathbf{k}}\langle\mathbf{v}_{\mathbf{k}}(t)\rangle$, where S is the normalization area, $\mathbf{v}_{\mathbf{k}}(t) = \psi_{\mathbf{k}}^\dagger(t)\nabla_{\mathbf{k}}[\mathcal{H}_{\mathbf{k}}(t)/\hbar]\psi_{\mathbf{k}}(t)$ is the single-electron velocity operator, and $\langle\mathcal{M}\rangle = \text{Tr}(\rho_0\mathcal{M})$ is the canonical ensemble average of the operator \mathcal{M} in terms of the initial density matrix $\rho_0 = e^{-\mathcal{H}/k_{\text{B}}T}/\text{Tr}(e^{-\mathcal{H}/k_{\text{B}}T})$, which depends on the switching protocol as discussed later. The time evolution of $\mathbf{J}(t)$ is expressed by using the lesser Green’s function, $[\hbar G_{\mathbf{k}}^<(t, t)]_{\alpha\beta} = i\langle c_{\mathbf{k}\beta}^\dagger(t)c_{\mathbf{k}\alpha}(t)\rangle$. In this work, if we focus on a NESS, the system recovers time translational symmetry, i.e., $\mathcal{H}(t) = \mathcal{H}(t+\tau)$ with periodicity $\tau (= 2\pi/\Omega)$, and is thus governed by the Floquet theorem [31]. By considering the Floquet mode expansion of the Green’s function, $[\hbar G_{\mathbf{k}}^<(t, t)]_{\alpha\beta} = \sum_{m, n \in \mathbb{Z}} e^{-i(m-n)\Omega t} \int_{-\hbar\Omega/2}^{\hbar\Omega/2} d\hbar\omega [\hat{G}_{\mathbf{k}}^<(\omega)]_{\alpha\beta; mn}/2\pi$, we find the surface current

density $J_\mu(t) = \sum_{s \in \mathbb{N}} \text{Re}[\sigma_{\mu x}^s(E)Ee^{-is\Omega t}]$ ($\mu \in \{x, y\}$), where the s -th harmonics of the field-dependent dynamical longitudinal and Hall conductivities are given by

$$\text{Re}[\sigma_{xx}^s(E)] = \text{Im}[\tilde{\sigma}_+^s(E)], \quad (1)$$

$$\text{Im}[\sigma_{yx}^s(E)] = \text{Im}[\tilde{\sigma}_-^s(E)], \quad (2)$$

for the dissipative (incoherent) components, and

$$\text{Re}[\sigma_{yx}^s(E)] = \text{Re}[\tilde{\sigma}_+^s(E)], \quad (3)$$

$$\text{Im}[\sigma_{xx}^s(E)] = -\text{Re}[\tilde{\sigma}_-^s(E)], \quad (4)$$

for the reactive (coherent) components, and $\tilde{\sigma}_\pm^s(E)$ reads

$$\begin{aligned} \frac{\tilde{\sigma}_\pm^s(E)}{\sigma_0} &= -2\frac{E_0}{E} \left(\frac{v\hbar}{\Delta}\right)^2 \frac{1}{S} \sum_{\mathbf{k}} \sum_{n \in \mathbb{Z}} \int_{-\hbar\Omega/2}^{\hbar\Omega/2} d\hbar\omega \\ &\times \left\{ [\hat{G}_{\mathbf{k}}^<(\omega)]_{\uparrow\downarrow; n+s, n} \pm [\hat{G}_{\mathbf{k}}^<(\omega)]_{\uparrow\downarrow; n, n+s} \right\}. \end{aligned} \quad (5)$$

Here, $E_0 = \Delta^2/(ev\hbar)$ defines a natural scale of maximum field strength in our problem at which Zener breakdown occurs [32], and $\sum_{\mathbf{k}} = S(2\pi v\hbar)^{-2} \int_{\Delta/2}^{\mathcal{E}_c} d\mathcal{E}_{\mathbf{k}} \mathcal{E}_{\mathbf{k}} \int_0^{2\pi} d\varphi_{\mathbf{k}}$ with $\varphi_{\mathbf{k}} = \tan^{-1}(k_y/k_x)$ and \mathcal{E}_c being an ultraviolet energy cutoff for the Dirac model at the level of low-energy effective theory.

Green’s function in the Keldysh-Floquet space.— Now, our main task boils down to finding the lesser Green’s function $\hat{G}_{\mathbf{k}}^<$ in Eq. (5), which can be achieved using the Keldysh-Floquet Green’s function formalism [33, 34]. In this formalism, the Keldysh contour is introduced in the time domain, since quantum states at remote past and future on a single time-ordered branch are not adiabatically connected to each other under nonequilibrium condition [35, 36]. Especially, regarding NESS, the contour-ordered Green’s function is mapped onto the Keldysh space, represented by a 2×2 matrix. This Keldysh space is further extended to include the Floquet space for systems satisfying the Floquet theorem.

The interacting Green’s function is governed by the Dyson equation, represented in the Keldysh-Floquet space as follows:

$$\begin{pmatrix} \hat{G}_{\mathbf{k}}^R & \hat{G}_{\mathbf{k}}^K \\ 0 & \hat{G}_{\mathbf{k}}^A \end{pmatrix}^{-1} = \begin{pmatrix} \hat{G}_{\mathbf{k}}^R & \hat{G}_{\mathbf{k}}^K \\ 0 & \hat{G}_{\mathbf{k}}^A \end{pmatrix}^{-1} - \begin{pmatrix} \hat{\mathcal{V}} & 0 \\ 0 & \hat{\mathcal{V}} \end{pmatrix}. \quad (6)$$

On the left-hand side of Eq. (6), the retarded, advanced, and Keldysh components are defined by $[\hat{G}_{\mathbf{k}}^\gamma(\omega)]_{\alpha\beta; mn} = \int dt e^{i(\omega+m\Omega)t} \int dt' e^{-i(\omega+n\Omega)t'} [G_{\mathbf{k}}^\gamma(t, t')]_{\alpha\beta}$ ($\gamma = R, A, K$), where $[\hbar G_{\mathbf{k}}^{R, A}(t, t')]_{\alpha\beta} = \mp i\Theta(\pm t \mp t') \langle \{c_{\mathbf{k}\alpha}(t), c_{\mathbf{k}\beta}^\dagger(t')\} \rangle$, $[\hbar G_{\mathbf{k}}^K(t, t')]_{\alpha\beta} = -i\langle [c_{\mathbf{k}\alpha}(t), c_{\mathbf{k}\beta}^\dagger(t')] \rangle$, and $-\Omega/2 \leq \omega < \Omega/2$. In the right-hand side of Eq. (6), the first term describes the initial NESS at $t = 0$ after transient effects have washed out, and the second term corresponds to the perturbation defined by $(\hat{\mathcal{V}})_{mn} = \tau^{-1} \int_0^\tau dt e^{i(m-n)\Omega t} \mathcal{V}(t) = -i(\mathcal{V}_0/2)\tau_x(\delta_{m, n+1} - \delta_{m, n-1})$. Provided that the initial NESS is known, the interacting

Green's function can be found by numerically inverting Eq. (6). Then, the result is inserted into Eq. (5) through the relation $\hat{G}_{\mathbf{k}}^< = (\hat{G}_{\mathbf{k}}^K - \hat{G}_{\mathbf{k}}^R + \hat{G}_{\mathbf{k}}^A)/2$.

In Eq. (6), the initial NESS was not specified yet. We assume that the optical field is adiabatically switched on with the switch-on time τ_s long enough compared with other time scales in the system, so as to restore the condition of thermal equilibrium at $t = 0$ [37]. Under this condition, the initial NESS is described by the equilibrium Green's function with the components: $\hat{G}_{\mathbf{k}}^\gamma(\omega) = \mathcal{U}_{\mathbf{k}} \hat{g}_{\mathbf{k}}^\gamma(\omega) \mathcal{U}_{\mathbf{k}}^\dagger$ ($\gamma = R, A, K$), where $[\hat{g}_{\mathbf{k}}^R(\omega)]^{-1} = \mathbb{I}_2 \otimes [(\hbar\omega + i\eta)\mathbb{I}_\infty + \hbar\hat{\Omega}] - \mathcal{E}_{\mathbf{k}}\tau_z \otimes \mathbb{I}_\infty$ and $[\hat{g}_{\mathbf{k}}^A(\omega)] = [\hat{g}_{\mathbf{k}}^R(\omega)]^\dagger$. $\hat{g}_{\mathbf{k}}^K$, satisfying the fluctuation-dissipation relation [36], is given by $\hat{g}_{\mathbf{k}}^K(\omega) = [\hat{g}_{\mathbf{k}}^R(\omega) - \hat{g}_{\mathbf{k}}^A(\omega)]\mathbb{I}_2 \otimes [\mathbb{I}_\infty - 2\hat{\mathcal{F}}(\omega)]$. Here, \mathbb{I}_n is the $n \times n$ identity matrix, η is the band broadening width due to elastic scattering of electrons, $(\hat{\Omega})_{mn} = n\Omega\delta_{mn}$, and $[\hat{\mathcal{F}}(\omega)]_{mn} = f_{\text{FD}}(\omega + n\Omega)\delta_{mn}$ with $f_{\text{FD}}(\omega) = (e^{\hbar\omega/k_B T} + 1)^{-1}$. The unitary operator $\mathcal{U}_{\mathbf{k}} = [\sin(\vartheta_{\mathbf{k}}/2)(\cos\varphi_{\mathbf{k}}\tau_x + \sin\varphi_{\mathbf{k}}\tau_y) + \cos(\vartheta_{\mathbf{k}}/2)\tau_z] \otimes \mathbb{I}_\infty$ transforms the original spin representation of $\mathcal{H}_{\mathbf{k}}$ into the band representation, with $\vartheta_{\mathbf{k}} = \cos^{-1}[\Delta/(2\mathcal{E}_{\mathbf{k}})]$.

Linear-response and near-resonance regimes.— Our formalism provides a generic framework to investigate the dynamical response of massive Dirac electrons to strong optical fields. Before applying our theory to the full non-perturbative regime, here we consider in particular (i) the linear-response and (ii) the near-resonance coherent regimes, and see whether our framework reproduces established results in these well-known limits.

First, we are able to recover the linear-response result when $\mathcal{V}_0 \ll \Delta$. In this regime, Eq. (6) can be expanded analytically up to the linear order in \mathcal{V}_0 , and we recover the Kubo formula result for dynamical conductivity [21] (see Supplementary Material for details). In Fig. 1(a), we also numerically confirm that the linear-response behavior of the dynamical Hall conductivity is recovered as the optical field strength is decreased (the reference plot of the Kubo formula result is indicated by the red solid line) [39]. In the low-frequency regime, we notice that the one-half Hall quantization remains robust against weak fields.

Secondly, we examine the near-resonance coherent regime, where the optical frequency is close to the band gap with the detuning $\delta (= \Delta - \hbar\Omega)$ satisfying $\Delta \gg \delta \gg \eta$. For the Dirac model, a theory based on the Bloch equation has been developed within the rotating wave approximation (RWA) [40] (see Supplementary Material for details). The result for the dynamical Hall conductivity from this theory is plotted in Fig. 1(b) as the red solid line. For weak fields ($E/E_0 \lesssim 0.2$), as η decreases below δ approaching the coherent regime ($\eta \rightarrow 0$), we find close agreement between the Keldysh-Floquet and the Bloch-RWA results. This regime corresponds to weak coupling with $\lambda \ll 1$. On the other hand, for stronger fields ($E/E_0 \gtrsim 0.2$), the Keldysh-Floquet result differs

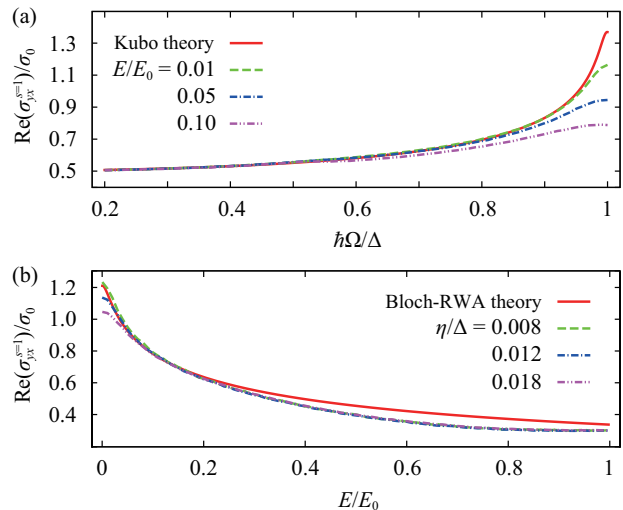


FIG. 1: Comparison of the dynamical Hall conductivity obtained by our theory with the counterpart (a) by the Kubo theory in the linear-response regime; (b) by the Bloch theory in the rotating wave approximation (RWA) near resonance. In (a), we set $\eta/\Delta = 0.01$ with varying E ; in (b), $\hbar\Omega/\Delta = 0.99$, or equivalently the detuning $\delta/\Delta = 1 - \hbar\Omega/\Delta = 0.01$, with varying η . In both (a) and (b), we have common parameters $k_B T/\Delta = 0.02$ and $\mathcal{E}_c/\Delta = 10$.

noticeably from the Bloch-RWA result, because n -photon excitation processes ($n \geq 2$) that becomes important at strong fields are ignored in the RWA [41], but are exactly captured in the Keldysh-Floquet approach.

Dynamical QAHE.— Our main interest in this work is to investigate the robustness and the dynamical breakdown of the QAHE without restricting ourselves to the linear-response or near-resonance coherent regimes. Here, we focus our discussion on $\text{Re}[\sigma_{xx}^{s=1}(E)]$ and $\text{Re}[\sigma_{yx}^{s=1}(E)]$, which are sufficient to capture the QAHE in the low-frequency regime. Figure 2 shows the dynamical breakdown of the QAHE as a function of optical field strength for different frequencies. Both the longitudinal and Hall conductivities exhibit a consistent pattern underlain by the following two main features. First, there is a clear signature for the robustness of the half-quantized Hall regime. In Fig. 2(b), for $\hbar\Omega/\Delta = 0.2$, low enough to capture the QAHE, the regime is robust up to a threshold optical field strength $E_{th}/E_0 \approx 0.12$. For $E < E_{th}$, the longitudinal counterpart is suppressed, and the generalized Hall angle θ_H , which is defined by $\tan^{-1}[\text{Re}(\sigma_{yx}^{s=1})/\text{Re}(\sigma_{xx}^{s=1})]$, attains the maximum value $\pi/2$ [see Fig. 2(a) and (c)]. Secondly, in the regime of $E > E_{th}$, the QAHE dynamically collapses, and the conductivities exhibit an oscillatory behavior, which becomes more prominent with decreasing optical field frequency or increasing field strength.

In Fig. 3, we show the full dependence of the dynamical Hall conductivity on both the optical frequency and field strength. The lower left corner of the plot

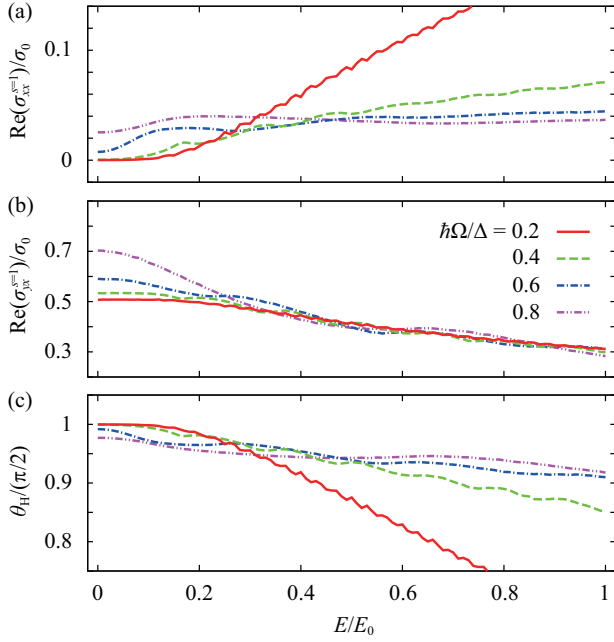


FIG. 2: Dynamical breakdown of the one-half QAHE. Each panel shows (a) the dynamical longitudinal conductivity, (b) the dynamical Hall conductivity, and (c) the generalized Hall angle as a function of optical field strength E for some values of optical frequency Ω . Here, we used the parameters $k_B T/\Delta = 0.02$, $\eta/\Delta = 0.01$, and $\mathcal{E}_c/\Delta = 10$.

labeled by “QAHE” corresponds to the low-field adiabatic regime in which the quantized Hall conductivity remains robust. The region with $E < E_{th} \approx 0.12E_0$ and $\hbar\Omega \in (0, \Delta)$ corresponds to the linear-response regime where the Kubo theory is valid; whereas the region with $\hbar\Omega \approx \Delta$ and $E \in (0, E_0)$ is approximately captured by the Bloch-RWA theory when multiphoton processes are ignored. We observe that the oscillatory behavior is most prominent in the upper left corner of Fig. 3, where $\hbar\Omega/\Delta \approx 0.2$ and $E/E_0 \lesssim 1$. This regime with low frequency and high electric field is characterized by a strong light-matter coupling, since $\lambda = (E/E_0)/(\hbar\Omega/\Delta)^2 \gg 1$. Numerical calculations in this regime is challenging because of the large number of Floquet modes involved due to a small frequency. To understand the behavior in this regime, we treat the time-independent part of the Hamiltonian $\mathcal{H}_{\mathbf{k}}$ as a perturbation [42], valid when $\mathcal{V}_0 \gg \mathcal{E}_{\mathbf{k}} \geq \Delta/2$. To linear order in $\mathcal{E}_{\mathbf{k}}/\mathcal{V}_0$, we find that $\text{Re}[\sigma_{yx}^{s=1}(E)] \propto \sum_{n \in \mathbb{N}} \mathcal{Q}_n \mathcal{W}_n$, where \mathcal{Q}_n and \mathcal{W}_n are weight functions corresponding to the Floquet state with n -photon excitations ($n \geq 1$), labeled by “ \mathcal{F}_n ” in Fig. 3:

$$\mathcal{Q}_n = \int_{-\infty}^{\infty} d\tilde{\omega} \int_{-\infty}^{\infty} d\tilde{\omega}' \mathcal{P} \frac{1}{\tilde{\omega}' - \tilde{\omega} + \Omega} \rho(\tilde{\omega}) \rho(\tilde{\omega}' + n\Omega) \times [f_{\text{FD}}(\tilde{\omega}) - f_{\text{FD}}(\tilde{\omega}' + n\Omega)], \quad (7)$$

$$\mathcal{W}_n = \frac{E_0}{E} \mathbb{J}_{n-1}(2\lambda) [\mathbb{J}_n(2\lambda) - \mathbb{J}_{n-2}(2\lambda)] (1 - \delta_{n,1}/2), \quad (8)$$

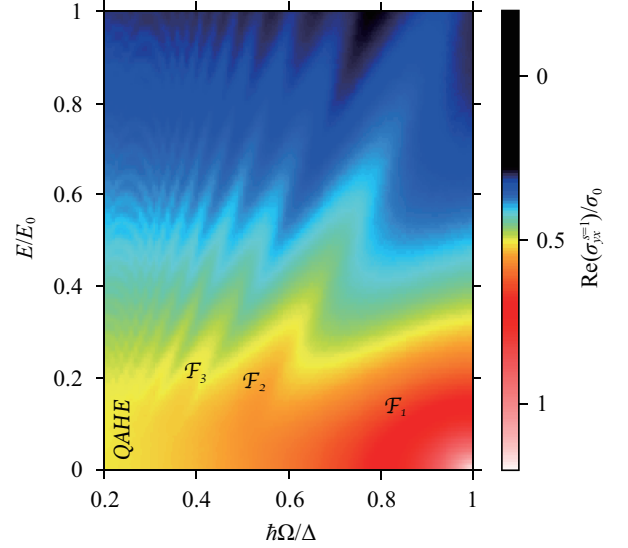


FIG. 3: Phase diagram for the dynamical Hall conductivity as a function of the optical frequency Ω and the optical field strength E . The right panel indicates the color legend for the dynamical Hall conductivity. “QAHE” indicates the QAHE phase, and “ \mathcal{F}_n ” ($n \in \mathbb{N}$) the Floquet state with n -photon excitations. Unassigned parameters are the same as in Fig. 2.

where \mathcal{P} stands for the principle value integral, $\rho(\tilde{\omega}) = -\text{Im} \sum_{\mathbf{k}} \sum_{\alpha \in \{\uparrow, \downarrow\}} [\hat{G}_{\mathbf{k}}^R(\omega)]_{\alpha\alpha; nn} / \pi$ is the time-averaged local density of states with $\tilde{\omega} = \omega + n\Omega$, and $\mathbb{J}_n(x)$ is the Bessel function of the first kind (see Supplementary Material for details). We note that this result is closely connected to the tunneling current formula under *A.C.* bias voltage in the Tien-Gordon theory [43]; in fact, the Hall conductivity with Eqs. (7)–(8) is in the form of the Kramers-Kronig counterpart of the Tien-Gordon tunneling conductivity. Our numerical results show that the field dependence of \mathcal{Q}_n is insignificant. Instead, the main effect is captured in the asymptotic form of \mathcal{W}_n for $\lambda \gg 1$,

$$\mathcal{W}_n \approx \frac{1}{2\pi} \left[(-1)^n + \frac{1}{2} \delta_{n,1} \right] \frac{E_0 \cos(4\lambda)}{E \lambda}, \quad (9)$$

from which we see that the Hall current oscillates with the optical field strength E/E_0 at a frequency $\sim (\Delta/\hbar\Omega)^2$. The oscillation frequency is therefore a direct probe of the light-matter coupling λ , with more frequent oscillations characterizing a stronger coupling.

For bismuth-based TIs with Dirac velocity $v \approx 5 \times 10^5 \text{ ms}^{-1}$ and magnetically-induced gap $\Delta = 0.02 - 0.2 \text{ eV}$ [14–16, 26, 27], we estimate that the required optical frequency and field strength for observing coherent oscillations of the Hall conductivity are $\Omega < 30.39 - 303.9 \text{ THz}$ and $E \lesssim 1.215 - 121.5 \text{ MVm}^{-1}$, which are well within current experimental accessibility. The dynamical Hall conductivity in the TI film can be measured indirectly through magneto-optical Faraday and Kerr rotations, or directly in a standard Hall measurement geometry illu-

minated with the linear polarization of the normally incident light parallel to the length of the Hall bar. In addition to TIs, graphene or bilayer graphene doped with noble metal atoms offer an alternate class of systems with a band gap and associated topological Hall transport [12, 44]. In this scenario, the valley degrees of freedom give rise to a quantized valley Hall conductivity. Illuminated by a strong optical field, dynamical valley Hall currents will be generated in the transverse direction, which can be measured in a nonlocal transport geometry [45–47].

In summary, we have developed a theory for the dynamical quantum anomalous Hall effect driven by intense optical fields. Our theory addresses the question of the robustness of topological Hall quantization in the nonlinear electric field regime, and predicts a collapse of Hall quantization at high fields accompanied by coherent conductivity oscillations as a function of optical field strength. Our work sheds light on the problem of the nonequilibrium dynamical response of topological phases under a strong optical field, and our findings should offer new insights in nonequilibrium topological states particularly in the low-frequency, adiabatic regime.

This work is supported from a startup fund of the University of Alabama.

-
- [1] M. Z. Hasan and C. L. Kane, Colloquium: Topological insulators, *Rev. Mod. Phys.* **82**, 3045 (2010).
- [2] X.-L. Qi and S.-C. Zhang, Topological insulators and superconductors, *Rev. Mod. Phys.* **83**, 1057 (2011).
- [3] T. Oka and H. Aoki, Photovoltaic Hall effect in graphene, *Phys. Rev. B* **79**, 081406(R) (2009).
- [4] N. H. Lindner, G. Rafael, and V. Galitski, Floquet topological insulator in semiconductor quantum wells, *Nat. Phys.* **7**, 490 (2011).
- [5] L. Jiang, T. Kitagawa, J. Alicea, A.R. Akhmerov, D. Pekker, G. Refael, J. I. Cirac, E. Demler, M. D. Lukin, and P. Zoller, Majorana Fermions in Equilibrium and in Driven Cold-Atom Quantum Wires, *Phys. Rev. Lett.* **106**, 220402 (2011).
- [6] G. Liu, N. Hao, S.-L. Zhu, and W. M. Liu, Topological superfluid transition induced by a periodically driven optical lattice, *Phys. Rev. A* **86**, 013639 (2012).
- [7] R. Wang, B. Wang, R. Shen, L. Sheng, and D. Y. Xing, Floquet Weyl semimetal induced by off-resonant light, *Europhys. Lett.* **105**, 17004 (2014).
- [8] C.-K. Chan, P. A. Lee, K. S. Burch, J. H. Han, and Y. Ran, When Chiral Photons Meet Chiral Fermions: Photoinduced Anomalous Hall Effects in Weyl Semimetals, *Phys. Rev. Lett.* **116**, 026805 (2016).
- [9] C.-X. Liu, S.-C. Zhang, and X.-L. Qi, The Quantum Anomalous Hall Effect: Theory and Experiment, *Annu. Rev. Condens. Matter Phys.* **7**, 301 (2016).
- [10] R. Yu, W. Zhang, H.-J. Zhang, S.-C. Zhang, X. Dai, and Z. Fang, Quantized Anomalous Hall Effect in Magnetic Topological Insulators, *Science* **329**, 61 (2010).
- [11] Z. Qiao, S. A. Yang, W. Feng, W.-K. Tse, J. Ding, Y. Yao, J. Wang, and Q. Niu, Quantum anomalous Hall effect in graphene from Rashba and exchange effects, *Phys. Rev. B* **82**, 161414 (2010).
- [12] W.-K. Tse, Z. Qiao, Y. Yao, A. H. MacDonald, and Q. Niu, Quantum anomalous Hall effect in single-layer and bilayer graphene, *Phys. Rev. B* **83**, 155447 (2011).
- [13] C.-X. Liu, X.-L. Qi, X. Dai, Z. Fang, and S.-C. Zhang, Quantum Anomalous Hall Effect in $\text{Hg}_{1-y}\text{Mn}_y\text{Te}$ Quantum Wells, *Phys. Rev. Lett.* **101**, 146802 (2008).
- [14] C.-Z. Chang, J. Zhang, X. Feng, J. Shen, Z. Zhang, M. Guo, K. Li, Y. Ou, P. Wei, L.-L. Wang, Z.-Q. Ji, Y. Feng, S. Ji, X. Chen, J. Jia, X. Dai, Z. Fang, S.-C. Zhang, K. He, Y. Wang, L. Lu, X.-C. Ma, and Q.-K. Xue, Experimental Observation of the Quantum Anomalous Hall Effect in a Magnetic Topological Insulator, *Science* **340**, 167 (2013).
- [15] C.-Z. Chang, W. Zhao, D. Y. Kim, H. Zhang, B. A. As-saf, D. Heiman, S.-C. Zhang, C. Liu, M. H. W. Chan, and J. S. Moodera, High-precision realization of robust quantum anomalous Hall state in a hard ferromagnetic topological insulator, *Nat. Mater.* **14**, 473 (2015).
- [16] X. Kou, L. Pan, J. Wang, Y. Fan, E. S. Choi, W.-L. Lee, T. Nie, K. Murata, Q. Shao, S.-C. Zhang, and K. L. Wang, Metal-to-insulator switching in quantum anomalous Hall states, *Nat. Commun.* **6**, 8474 (2015).
- [17] T. Morimoto and N. Nagaosa, Topological nature of nonlinear optical effects in solids, *Sci. Adv.* **2**, e1501524 (2016).
- [18] T. Morimoto and N. Nagaosa, Topological aspects of nonlinear excitonic processes in noncentrosymmetric crystals, *Phys. Rev. B* **94**, 035117 (2016).
- [19] T. Morimoto, S. Zhong, J. Orenstein, and J. E. Moore, Semiclassical theory of nonlinear magneto-optical responses with applications to topological Dirac/Weyl semimetals, *Phys. Rev. B* **94**, 245121 (2016).
- [20] K. W. Kim, T. Morimoto, and N. Nagaosa, Shift charge and spin photocurrents in Dirac surface states of topological insulator, *Phys. Rev. B* **95**, 035134 (2017).
- [21] W.-K. Tse and A. H. MacDonald, Giant Magneto-Optical Kerr Effect and Universal Faraday Effect in Thin-Film Topological Insulators, *Phys. Rev. Lett.* **105**, 057401 (2010).
- [22] J. Maciejko, X.-L. Qi, H. Dennis Drew, and S.-C. Zhang, Topological Quantization in Units of the Fine Structure Constant, *Phys. Rev. Lett.* **105**, 166803 (2010).
- [23] K. N. Okada, Y. Takahashi, M. Mogi, R. Yoshimi, A. Tsukazaki, K. S. Takahashi, N. Ogawa, M. Kawasaki, and Y. Tokura, Terahertz spectroscopy on Faraday and Kerr rotations in a quantum anomalous Hall state, *Nat. Commun.* **7**, 12245 (2016).
- [24] L. Wu, M. Salehi, N. Koirala, J. Moon, S. Oh, and N. P. Armitage, Quantized Faraday and Kerr rotation and axion electrodynamics of a 3D topological insulator, *Science* **354**, 1124 (2016).
- [25] V. Dziom, A. Shuvaev, A. Pimenov, G. V. Astakhov, C. Ames, K. Bendias, J. Böttcher, G. Tkachov, E. M. Hankiewicz, C. Brüne, H. Buhmann, and L. W. Molenkamp, Observation of the universal magnetoelectric effect in a 3D topological insulator, arXiv:1603.05482.
- [26] Y. L. Chen, J.-H. Chu, J. G. Analytis, Z. K. Liu, K. Igarashi, H.-H. Kuo, X. L. Qi, S. K. Mo, R. G. Moore, D. H. Lu, M. Hashimoto, T. Sasagawa, S. C. Zhang, I. R. Fisher, Z. Hussain, Z. X. Shen, Massive Dirac Fermion on the Surface of a Magnetically Doped Topological In-

- ulator, *Science* **329**, 659 (2010).
- [27] L. Andrew Wray, S.-Y. Xu, Y. Xia, D. Hsieh, A. V. Fedorov, Y. S. Hor, R. J. Cava, A. Bansil, H. Lin, and M. Z. Hasan, A topological insulator surface under strong Coulomb, magnetic and disorder perturbations, *Nat. Phys.* **7**, 32 (2011).
- [28] H.-Z. Lu, W.-Y. Shan, W. Yao, Q. Niu, and S.-Q. Shen, Massive Dirac fermions and spin physics in an ultrathin film of topological insulator, *Phys. Rev. B* **81**, 115407 (2010).
- [29] Y. Wu and X. Yang, Strong-Coupling Theory of Periodically Driven Two-Level Systems, *Phys. Rev. Lett.* **98**, 013601 (2007).
- [30] E. K. Irish, Generalized Rotating-Wave Approximation for Arbitrarily Large Coupling, *Phys. Rev. Lett.* **99**, 173601 (2007).
- [31] M. Grifoni and P. Hänggi, Driven quantum tunneling, *Phys. Rep.* **304**, 229–354 (1998).
- [32] C. Zener, A theory of the electrical breakdown of solid dielectrics, *Proc. R. Soc. London, Ser. A* **145**, 523 (1934).
- [33] N. Tsuji, T. Oka, and H. Aoki, Nonequilibrium Steady State of Photoexcited Correlated Electrons in the Presence of Dissipation, *Phys. Rev. Lett.* **103**, 047403 (2009).
- [34] W.-R. Lee and K. Park, Dielectric breakdown via emergent nonequilibrium steady states of the electric-field-driven Mott insulator, *Phys. Rev. B* **89**, 205126 (2014).
- [35] J. Rammer and H. Smith, Quantum field-theoretical methods in transport theory of metals, *Rev. Mod. Phys.* **58**, 323–359 (1986).
- [36] H. Haug and A.-P. Jauho, *Quantum Kinetics in Transport and Optics of Semiconductors*, 2nd ed. (Springer, Berlin, Germany, 2008).
- [37] Microscopically, such a task requires a rigorous treatment of the coupling nature between the system and thermal bath [38]. This difficulty is circumvented by the adiabatic switch-on condition, so that the initial NESS at $t = 0$ is adiabatically connected to the equilibrium state at $t \rightarrow -\infty$. No further assumption on the properties of optical fields (*e.g.*, frequency and field strength) is required to determine the fully interacting NESS via Eq. (6).
- [38] H.-P. Breuer and F. Petruccione, *The Theory of Open Quantum Systems* (Oxford University Press, Oxford, England, 2002).
- [39] To compensate for the cutoff-dependent correction $[1 - \Delta/(2\mathcal{E}_c)]$ to the Hall conductivity [40], in the final plots of our numerical results, we rescale σ_{yx}^s by the constant $[1 - \Delta/(2\mathcal{E}_c)]^{-1}$ so that the Hall conductivity in the limit of $\Omega \rightarrow 0$ approaches the exact half quantized value. This rescaling is necessary since a large $\mathcal{E}_c (\gg \Delta)$, which would ensure the correction factor approaches 1, is not practical in our intensive numerical calculations. In all of our results, we have ensured that σ_{yx}^s at $\hbar\Omega \ll \Delta$ and $E \ll E_0$ has converged to the theoretical value $(\sigma_0/2)[1 - \Delta/(2\mathcal{E}_c)]$ before rescaling.
- [40] W.-K. Tse, Coherent magneto-optical effects in topological insulators: Excitation near the absorption edge, *Phys. Rev. B* **94**, 125430 (2016).
- [41] In the RWA, only $n = 1$ single-photon processes are included. This is because higher order $n \geq 2$ resonant transitions require virtual transitions to intermediate states, and the counter-rotating terms that correspond to such virtual transition processes are ignored.
- [42] G. Platero and R. Aguado, Photon-assisted transport in semiconductor nanostructures, *Phys. Rep.* **395** 1–157 (2004).
- [43] P. K. Tien and J. P. Gordon, Multiphoton Process Observed in the Interaction of Microwave Fields with the Tunneling between Superconductor Films, *Phys. Rev.* **129**, 647–651 (1963).
- [44] J. Ding, Z. Qiao, W. Feng, Y. Yao, and Q. Niu, Engineering quantum anomalous/valley Hall states in graphene via metal-atom adsorption: An ab-initio study, *Phys. Rev. B* **84**, 195444 (2011).
- [45] R. V. Gorbachev, J. C. W. Song, G. L. Yu, A. V. Kretinin, F. Withers, Y. Cao, A. Mishchenko, I. V. Grigorieva, K. S. Novoselov, L. S. Levitov, and A. K. Geim, Detecting topological currents in graphene superlattices, *Science* **346**, 448 (2014).
- [46] M. Sui, G. Chen, L. W. Shan, D. Tian, K. Watanabe, T. Taniguchi, X. Jin, W. Yao, D. Xiao, and Y. Zhang, Gate-tunable topological valley transport in bilayer graphene, *Nat. Phys.* **11**, 1027 (2015).
- [47] Y. Shimazaki, M. Yamamoto, I. V. Borzenets, K. Watanabe, T. Taniguchi, and S. Tarucha, Generation and detection of pure valley current by electrically induced Berry curvature in bilayer graphene, *Nat. Phys.* **11**, 1032 (2015).